BJR https://doi.org/10.1259/bjr.20220034

Received: 05 January 2022 | Accepted: 22 March 2022 | Published online: 02 May 2022

Cite this article as:
Golay X, Ho M-L. Multidelay ASL of the pediatric brain. *Br J Radiol* (2022) 10.1259/bjr.20220034.

REVIEW ARTICLE

Multidelay ASL of the pediatric brain

[1]XAVIER GOLAY, PhD and [2]MAI-LAN HO, MD

[1]MR Neurophysics and Translational Neuroscience, UCL Queen Square Institute of Neurology London, London, England, UK
[2]Radiology, Nationwide Children's Hospital and The Ohio State University, Columbus, OH, USA

Address correspondence to: Dr Mai-Lan Ho
E-mail: *ho.538@osu.edu;mailanho@gmail.com*

ABSTRACT:

Arterial spin labeling (ASL) is a powerful noncontrast MRI technique for evaluation of cerebral blood flow (CBF). A key parameter in single-delay ASL is the choice of postlabel delay (PLD), which refers to the timing between the labeling of arterial free water and measurement of flow into the brain. Multidelay ASL (MDASL) utilizes several PLDs to improve the accuracy of CBF calculations using arterial transit time (ATT) correction. This approach is particularly helpful in situations where ATT is unknown, including young subjects and slow-flow conditions. In this article, we discuss the technical considerations for MDASL, including labeling techniques, quantitative metrics, and technical artefacts. We then provide a practical summary of key clinical applications with real-life imaging examples in the pediatric brain, including stroke, vasculopathy, hypoxic-ischemic injury, epilepsy, migraine, tumor, infection, and metabolic disease.

INTRODUCTION

Arterial spin labeling (ASL) is a powerful noncontrast MRI technique for evaluation of cerebral blood flow (CBF). A key parameter in single-delay ASL is the choice of postlabel delay (PLD), which refers to the timing between the labeling of arterial free water and measurement of flow into the brain. Multidelay ASL (MDASL) utilizes several PLDs to improve the accuracy of CBF calculations using arterial transit time (ATT) correction. This approach is particularly helpful in situations where ATT is unknown, including young subjects and slow-flow conditions. In this article, we discuss the technical considerations for MDASL, including labeling techniques, quantitative metrics, and technical artefacts. We then provide a practical summary of key clinical applications with real-life imaging examples in the pediatric brain, including stroke, vasculopathy, hypoxic-ischemic injury, epilepsy, migraine, tumor, infection, and metabolic disease.

TECHNICAL CONSIDERATIONS

ASL is a non-contrast MRI technique used for the measurement of perfusion-related parameters.[1,2] In its most simple incarnation, it uses a preparation sequence upstream from the tissue of interest to invert the inflowing arterial water spins, and measures its arrival downstream. The rate at which the labeled blood is delivered to the tissue is called cerebral blood flow (CBF), measured in standard units of mL/min/100g. A typical ASL measurement consists of two consecutive acquisitions, the first one performed following labeling of the water spins, and the second without such labeling.[3] The subtraction of both acquisitions leads to a perfusion-weighted image, which needs further processing to be transformed into a quantitative CBF map. Importantly, the small inherent signal-to-noise ratio (SNR) of the method—a direct result of a subtraction between two acquisitions—can typically be compensated by using multiple repetitions or dedicated 3D-based acquisition methods, based on a combination of a rapid acquisition scheme (typically EPI or spiral imaging) with a fast-spin echo to rapidly cover large volumes.[3]

There are several ways to perform labeling of the arterial spins, and we will discuss the three most promising techniques in the brain. The first and most intuitive approach is called pulsed arterial spin labeling or PASL, and consists of positioning a large inversion volume upstream from the tissue of the brain, typically covering the basal portion of the skull and part of the neck (Figure 1a).[4,5] With this method, all spins in the arteries within this volume will be inverted at once, and the perfusion measurement will typically be performed after a certain postlabel delay (*PLD*) or inversion time *TI* (Figure 1b). Finally, to control the exact timing of the labeling pulse, extra saturation volumes can be added after a time TI_1.[6] A second method involves repetitively applying a series of small volumes, forming a thin labelling plane of typically about 1 cm in thickness over a relatively long time, using reduced flip angles in a method dubbed pseudocontinuous arterial spin labeling or pCASL

Figure 1. Geometrical representation (a,c,e) and pulse sequence diagrams (b,d,f) for various ASL labeling schemes. Labeling components of pulse sequences are shown in red. For PASL (a), labeling is volume selective and occurs in a single instant (b). The labeling duration is set by the additional saturation pulse applied so as to cut off the tail of the labeled blood bolus. The time *TI* is selected to allow the labeled spins to enter into the acquisition volume. For pCASL, the labeling volume is restricted to a thick plane (c), applied over a long labeling duration *t* (d). A corresponding postlabel delay (*PLD*) is included to allow the labeled spins to clear the intravascular space. For velocity-selective ASL (VSASL), the pulse sequence includes a saturation pulse, and two labeling modules (also applied over a very short amount of time), which are non-spatially selective, but will select all the flowing spins (red in (e)). These can then be detected after a post-labelling delay (PLD) (f), in a way similar to pCASL (d).

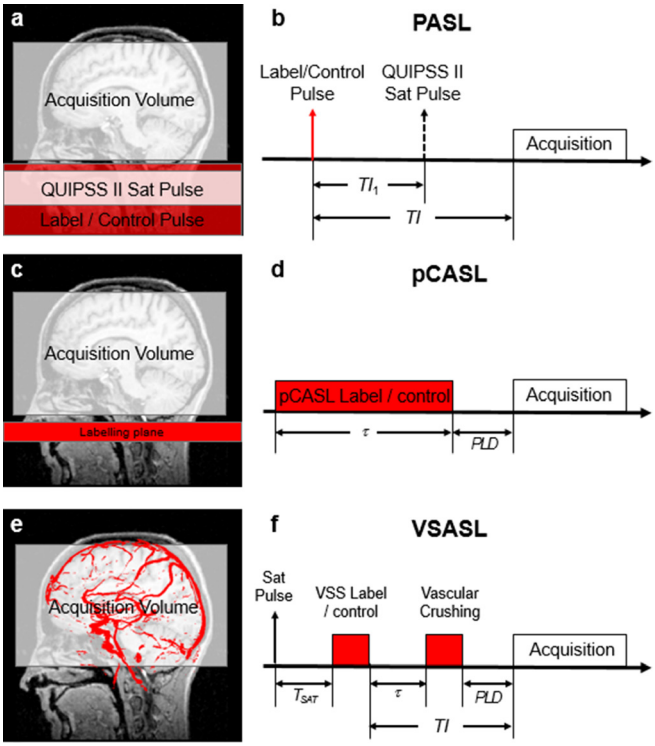

(Figure 1c & d).[7] This method works by inverting the spins while they progress through these small volumes in a pseudo adiabatic fashion. It has several advantages over the PASL method, in that it allows for a much longer bolus of arterial labeling and ensures that all spins are labeled as close to the tissue of interest as possible, thereby theoretically increasing the SNR of the ASL sequence by a factor $\sqrt{2}$.[3] Finally, a third method has more recently been developed, based on a completely different labeling scheme, in which arterial water spins are labeled (either saturated or inverted) based on their velocities (Figure 1e & f). This method is therefore dubbed velocity-selective arterial spin labeling, or VSASL.[8] The main advantage of this ASL sequence over the other two is that spins can be labeled much closer to the tissue of interest, thereby drastically reducing the arterial transit time. [Figure 1]

A consensus paper by the ISMRM Perfusion Study Group and European Consortium for ASL in Dementia[3] describes in more detail all aspects of the first two techniques for both acquisition and processing steps to produce CBF maps. It also provides a clear set of parameters to be used to get a good first approximation of CBF measurements in multiple clinical conditions. Briefly, the measured difference image $\Delta M = M_C - M_L$ needs to be scaled by a proton-density map of the tissue M_0 and a series of other parameters to produce a CBF map using the following equations, depending on whether PASL or pCASL is used:

$$CBF = 6000 \frac{\lambda}{2\alpha} \frac{\Delta M}{M_0} \frac{e^{\frac{TI}{T_{1b}}}}{TI_1} [\text{mL/min/100g}], \text{ for PASL [1]}$$

$$CBF = 6000 \frac{\lambda}{2\alpha} \frac{\Delta M}{M_0} \frac{e^{\frac{PLD}{T_{1b}}}}{T_{1b}\left(1-e^{-\frac{\tau}{T_{1b}}}\right)} [\text{mL/min/100g}], \text{ for PCASL [2]}$$

In both equations, the factor 6000 allows to set the units in the historical values of mL per min per 100g of tissue. With volumes in both the numerator and denominator, the resulting units are in units of [1/Time], which is by definition a rate. In addition, both equations are very similar and differ only in the last part. The term $\frac{\lambda}{2\alpha}$ scales the blood flow by the blood : brain partition coefficient λ and the labeling efficiency α. The main data being scaled is the $\frac{\Delta M}{M_0}$ term, representing the difference between both images normalized by the proton density-weighted image M_0 . In both equations, T_{1b} is the blood T_1 relaxation time, while *TI* and TI_1 are defined in Figure 1b an *PLD* and τ in Figure 1d.

One of the main assumptions for these equations to be valid, and for images to truly reflect the amount of blood delivered to the brain, is that the PLD needs to be long enough for spins to be delivered via the microvasculature into the tissue.[9] This is the greatest problem with simple single-delay ASL methods: while this assumption can be accepted in general for most clinical applications *without* vessel disease, it is often incorrect in subjects of young or old age and various slow-flow conditions, *e.g.* arterial occlusion or abnormal circulation.[10] For that reason, it can be preferable to use multiple acquisitions at various PLDs to completely characterize the whole dynamics of the arterial blood bolus when it passes through the brain. This approach is referred to as multidelay ASL (MDASL), for which each MRI vendor has developed a slightly different labeling approach. Of note, VSASL is not typically used with multiple delays, as labeling is already performed very close to the tissue of interest throughout the brain.

Labeling techniques

Look-Locker technique

The Look-Locker encoding method was the first to be developed[11,12] and is based on a simple PASL scheme, followed by a series of equally spaced acquisitions, using a small flip angle together with a multislice gradient echo EPI readout. Generally, this approach is relatively rapid as it allows for acquisition of multiple *TI*s in one acquisition, but presents with significant drawbacks compared to standard ASL sequences: 1) much lower SNR, due to a small flip angle readout to save magnetization until later time points; 2) SNR is further reduced by a readout that is

Figure 2. Multidelay ASL images acquired using the Look-Locker technique (a), Multi-TI technique (c), and Hadamard encoding (e). The pulse sequence timings are represented on the right hand side. For the Look-Locker technique (b), a single acquisition is needed to acquire all images, using a small flip angle α. For the Multi-TI technique, the same sequence is basically repeated multiple times after various inversion times TI_n. Finally in the case of Hadamard encoding (here as an example using Walsh-ordered encoding steps[14]), for each acquisition, a different series of label (red) and control (white) steps is applied, and a numerical algorithm allows to reconstruct individual perfusion-weighted images at different ΔTIs. Figure 2c, courtesy of M. Guenther. Figure 2e adapted from[14] with permission.

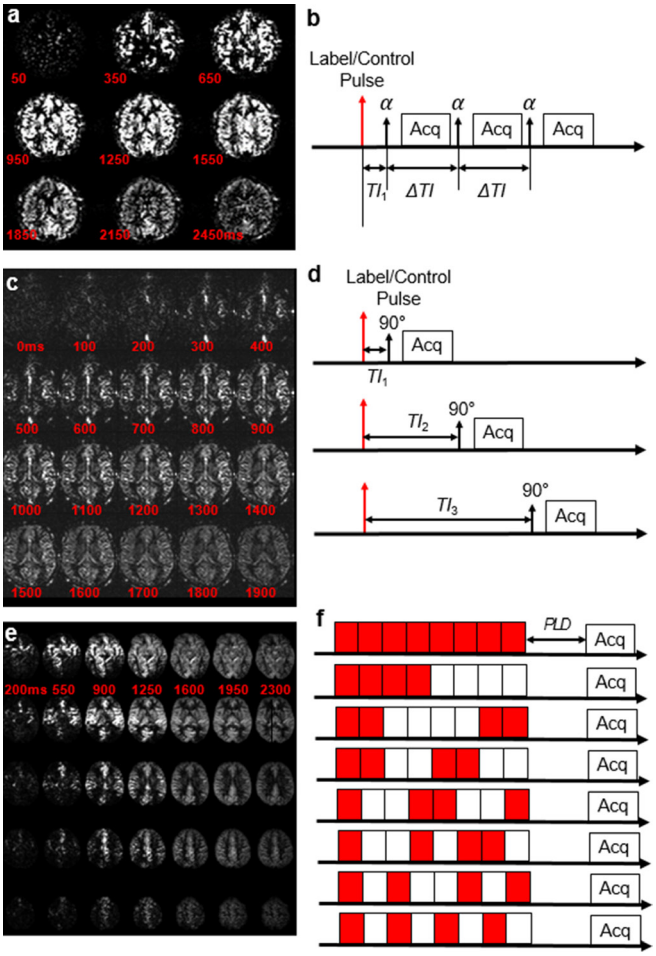

typically multislice rather than 3D; 3) limited imaging volume, due to the trade-off between number of inversion times and coverage. A key advantage is complete kinetic characterization of the bolus, including bolus arrival time (BAT) to tissue, which enables accurate quantification.[13] This method is currently provided by *Philips Healthcare* (Best, Netherlands). It usually requires up to 50 averages to provide satisfactory SNR, which with a typical TR of 3 s, results in a total scan time of 5 min. [Figure 2a–b]

Multi-TI

Another way of implementing MDASL is by acquiring several single-delay ASL images with either a PASL or pCASL labeling scheme.[15] As 3D readouts are much more SNR-effective, this method does not require many repetitions for each *TI*.[16] Potential disadvantages of this sequence are: 1) since each measurement is completely independent, there may be subject motion between different *TI*s; 2) generally, it takes up to 1 min per single *TI* to achieve adequate SNR, which forces a compromise between SNR and number of inversion times. This method also allows for quantitative assessment of the BAT.[15] This method is implemented by *Siemens Healthineers* (Enrlangen, Germany) using either labeling and 3D-GRASE readout. [Figure 2c–d]

Hadamard encoding

A final approach to MDASL is Hadamard encoding,[14] which takes advantage of the multiple acquisitions required for sufficient SNR to vary the labeling scheme during successive averages. Mathematical processing can then be used to synthesize post-hoc ASL images at various inversion times. Because of the improved SNR of this method over standard multi-TI,[14] the entire sequence can usually be contained within a few minutes. This method seems to provide the best compromise to maximize both coverage and number of delays. However, the data require special pre-processing, which increases the risks of failure if any of the datasets is corrupted. This technique is implemented by *GE Healthcare* (Chicago, IL), with the bolus split into seven subboli of different temporal labelling and control sequences. A minimum of 8 averages is needed to reconstruct all images with varying PLDs. Each of the eight images can be added or subtracted in a combinatorial fashion to recreate ASL-weighted images at various PLDs. For example, the ASL-weighted image corresponding to bolus seven can be reconstructed from all data using the following equation:

$$\Delta M\left(bolus7\right) = Im1 - Im2 - Im3 + Im4 - Im5 + Im6 + Im7 - Im8 \quad [3]$$

[Figure 2e–f]

Quantitative metrics

While single-delay ASL permits assessment of CBF, MDASL enables calculation of several additional perfusion metrics. By following the bolus of labeled arterial blood through tissue, the arterial transit time (ATT) can be reported as the time in ms at which the signal ΔM appears in the tissue of interest. In single-delay ASL, perfusion-weighted signal can be absent or suboptimal depending on the choice of times *TI* or *PLD*. With MDASL, the acquisition of perfusion-weighted images at multiple time points enables calculation of an ATT-corrected CBF, in which some of the assumptions for Equations [1] and [2] are now fulfilled. Multiple methods can be utilized to fit the measured signal and calculate perfusion parameters using models[17,18] or model-free methods,[13] analogous to other clinical perfusion techniques such as dynamic susceptibility contrast (DSC).[19] ASL uses blood water as an endogenous tracer, which distributes freely throughout the entire tissue intravascular and extravascular space. Perfusion-weighted signal comes from the arterial vasculature, primarily the distal vascular tree within small

arterioles prior to reaching the capillary system. The majority of the labeled water is extracted on first passage, where it almost instantaneously exchanges with extravascular tissue water. More advanced models utilize arterial cerebral blood volume (ACBV) as a scaling factor in units of mL/100g.[13,17] Estimation of total cerebral blood volume (CBV) requires an endogenous or exogenous tracer, such as the gadolinium-based contrast agents used in DSC, to quantify signal from the intravascular space.[19]

TECHNICAL ARTEFACTS

MDASL considerably improves the accuracy and reproducibility of ASL in patient populations for which ATT is often unknown.[20–22] However, the more basic models for CBF calculation do not correct for intravascular signal, which can lead to incorrect overestimation of perfusion values due to the large signal present in arteries.[10] Many of the algorithms implemented on clinical platforms are indeed quite simple, such that the automatically generated perfusion values need to be assessed with caution. One of the main assumptions for the model equations to be valid, and for ASL images to truly reflect the amount of blood delivered to the brain, is that the PLD needs to be long enough for spins to arrive in the tissue of interest.[9] This is the greatest problem with single-delay ASL methods: while an average PLD assumption is acceptable for many clinical applications *without* vascular disease, it is often incorrect in subjects who are very young or old, as well as for slow-flow disorders, *e.g.* arterial stenosis or occlusion.[10] For that reason, it can be preferable to use multiple acquisitions at various PLDs to fully characterize the dynamic profile of the arterial blood bolus as it passes through the brain.

In MDASL, transit time correction weights CBF toward longer PLDs, and is therefore optimally utilized in conditions of slow flow.[23–27] In young children, particularly newborns and infants, the overall flow velocity is slow and it becomes difficult to estimate at what time a bolus of arterial blood will enter the brain.[28] Pathologic conditions such as stroke, vasculopathy, and hypoxic-ischemic injury can also decrease overall flow. The arterial transit artefact (ATA) is identified by the prolonged retention of spins within the arterial vasculature at PLDs when they should normally undergo capillary exchange.[29,30] The use of longer labels makes the MDASL approach very important for accurate flow quantification in steno-occlusive disorders. In situations involving elevated flow, *e.g.* ictal epilepsy or infection, transit time correction may artifactually mask perfusion differences. This quantification error can be minimized by utilizing more complex models that also account for ACBV.[17]

As for any clinical sequence, there are practical tradeoffs between time and information. Different techniques for MDASL may result in longer imaging times, or conversely lower SNR for the same imaging time since measurements are split between different PLDs. Other artefacts, such as head positioning, motion, and susceptibility, are analogous to single-delay ASL and can be further complicated by differences between individual acquisitions.[30–32] A number of protocol optimization techniques have been developed to reduce artefacts and improve contrast in MDASL.[33–41]

Figure 3. Arterial stroke. (a) Acute right MCA infarct with abrupt arterial cutoff and restricted diffusion (arrows). MDASL shows prolonged ATT with arterial transit artefact (arrows), indicating slow flow with attempted leptomeningeal collateralization. Transit time-corrected CBF is decreased (arrows) beyond the area of core infarct. This DWI-ASL mismatch indicates tissue at risk (ischemic penumbra), which can theoretically be rescued by early recanalization. In the absence of intervention, this region is likely to progress to completed infarct. (b) Subacute left MCA infarct, with edema evolving to encephalomalacia (arrows). MDASL shows minimal attempted collateralization with arterial transit artefact on ATT map and matched decrease in CBF (arrows). Transit time correction improves estimation of normal CBF and homogeneity across the field-of-view.

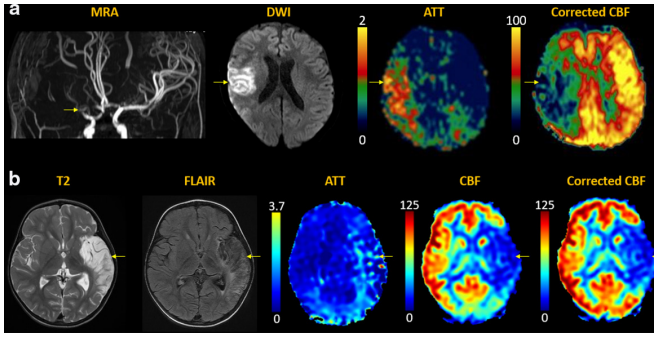

CLINICAL APPLICATIONS

Stroke

Acute stroke can be arterial or venous in aetiology. Arterial infarcts are caused by stenosis or occlusion of arteries supplying brain tissue, reducing cerebral blood flow and leading to energy failure with cytotoxic parenchymal injury. The severity of cerebral ischemia has been linked to ATA and CBF measurements on ASL,[42,43] and accuracy improves with multidelay approaches.[44–47] MDASL metrics have also been correlated with other perfusion imaging modalities including DSC MRI, computed tomography (CT) perfusion, single photon emission computed tomography (SPECT), and positron emission tomography (PET).[48–50] [Figure 3]

Venous infarcts result from thrombosis within the deep and/or superficial draining cerebral veins, including the dural venous sinuses. This results in outflow obstruction with blood-brain barrier disruption and vasogenic edema. Over time, rising tissue pressures can lead to parenchymal hemorrhage and secondary arterialization of stroke due to inflow impairment. On ASL, the "bright sinus" sign is a harbinger of trapped arterial spins proximal to the venous obstruction and can resolve following antithrombotic therapy.[51–53] MDASL helps to more accurately quantify perfusion metrics in the setting of slow flow. [Figure 4]

Vasculopathy

Moyamoya disease is an obliterative vasculopathy that causes progressive stenosis of cerebral vessels, most commonly the supraclinoid internal carotid arteries. When associated with a predisposing condition, such as neurofibromatosis, Down syndrome, sickle cell anaemia, or radiation, it is known as moyamoya

Figure 4. Venous stroke. (a) Acute venous infarct in patient with genetic malformations and coagulopathy. Bifrontal hematomas with layering fluid-blood levels, cortical and medullary venous thrombosis (arrows). MDASL with transit time correction shows elevated bifrontal ACBV and CBF, reflecting combined venous congestion and inflammation. (b) Chronic right anterior temporal hemorrhagic venous infarct (black asterisks) with thrombus in the right vein of Labbe and transverse sinus (arrows). MDASL shows decreased flow to the right anterior temporal lobe (white asterisks) with high venous signal in the transverse sinus (arrows). Transit time correction better quantifies flow to parenchyma.

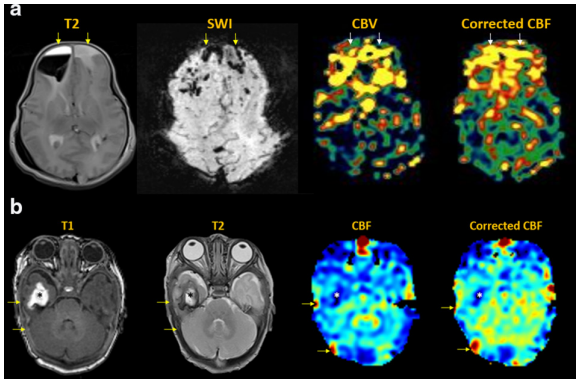

syndrome. Compensatory formation of multiple tortuous collateral vessels in the lenticulostriate, basal, and leptomeningeal circulations produces the characteristic "puff-of-smoke" appearance and "ivy sign" on angiography. By far, the most well-established application of MDASL is for quantifying perfusion in moyamoya patients, since flow through collateral vessels is far slower and more disorganized than in the normal arterial tree. As a result, short-delay ASL performed at conventional PLDs can yield a false-positive impression of ischemia. Longer labels are required to more accurately characterize the delayed inflow to brain parenchyma through collateral pathways.[54,55] In both preoperative and postoperative moyamoya patients, MDASL has been used to effectively characterize the degree of collaterals, tissue oxygenation, and cerebrovascular reserve (CVR) using acetazolamide or other vasoactive challenges.[56–58] These metrics have also been benchmarked against other perfusion imaging modalities.[59–63] [Figure 5]

Flow dynamics of other vasculopathies affecting the large, medium, and small vessels can also be characterized using MDASL. In comparison with the adult population, where such cases are often attributed to atherosclerosis or drug use, pediatric vasculopathies tend to be milder and in occasionally reversible. Major etiologies include connective tissue disorders, blood dyscrasias, inflammatory/infectious conditions, and vascular dysautoregulation.[64–72] [Figure 6]

Hypoxic-Ischemic injury

Hypoxic-ischemic injury (HII) has different imaging manifestations, depending on the severity and duration of cerebral flow compromise, as well as the timing of imaging after injury. Age of is also very important: children experience higher flow to actively developing brain regions, thus makes these areas

Figure 5. Moyamoya disease. (a) Right moyamoya disease with high-grade stenosis of the right carotid terminus and branches (yellow arrow), with incomplete reconstitution of distal branches via leptomeningeal collaterals. In this slow-flow condition, single-delay ASL markedly underestimates CBF. MDASL more accurately calculates CBF by accounting for slow flow through collateral vessels at long PLDs. At rest, there is increased ATT and decreased CBF in the right MCA distribution (arrows). Following intravenous acetazolamide challenge, maximal vasodilation induces diffusely elevated perfusion with reduction of ATT and CBF defects. This indicates intact residual cerebrovascular reserve, meaning that the patient is not at immediate risk of ischemia, and surgery can be delayed. (a) Down syndrome with right moyamoya post pial synangiosis (arrows). Chronic white matter ischemia and lacunar infarcts are present in the right hemisphere, with overlying enhancing leptomeningeal collaterals. seven consecutive PLDs demonstrate slow retrograde flow through the synangiosis (arrows) into the right MCA territory. There is progressive regional improvement in right hemispheric perfusion defects, with residual borderzone hypoperfusion. MDASL shows persistently increased ATT and decreased CBF to the right external vascular borderzones, better quantified after transit time correction. (b) Bilateral moyamoya disease with high-grade ICA occlusions, post bilateral synangiosis (arrows) communicating with leptomeningeal vessels. Multifocal lacunar infarcts are present, with numerous lenticulostriate and thalamoperforator moyamoya collaterals. MDASL shows patent synangioses with decreased ATT and increased CBF (arrows). Slow flow through synangiosis and collateral vessels is reflected in transit time-corrected CBF. There is residual hypoperfusion to the external vascular borderzones with elevated ATT and decreased CBF.

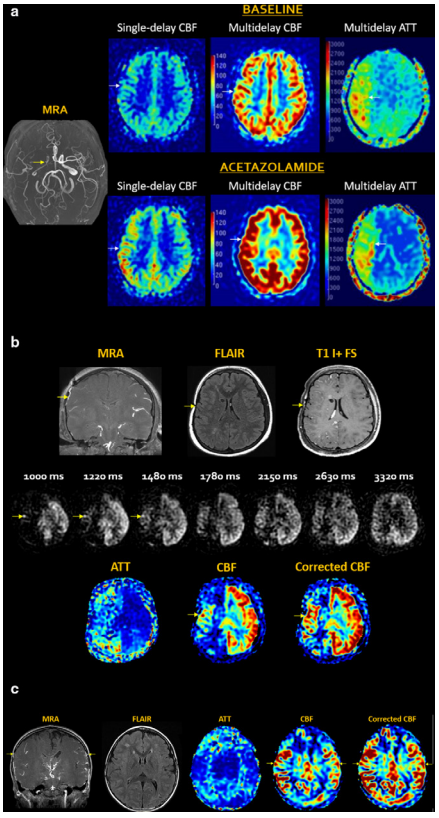

Figure 6. Other vasculopathies. (a) Sickle cell anaemia with scattered lacunar infarcts and radiating linear white matter FLAIR hyperintensities (yellow arrows). MDASL with transit time correction shows increased ATT and decreased CBF to the bilateral vascular watershed zones, between major arterial territories and within deep white matter (white arrows). (b) Posterior reversible encephalopathy with edema in the deep gray nuclei, parieto-occipital cortex and white matter (yellow arrows). MDASL shows increased ATT and decreased CBF to the bilateral posterior watershed zones with arterial transit artefact (white arrows). Transit time correction increases sensitivity for seizure-induced cortical hyperperfusion, with the watershed hypoperfusion areas less apparent.

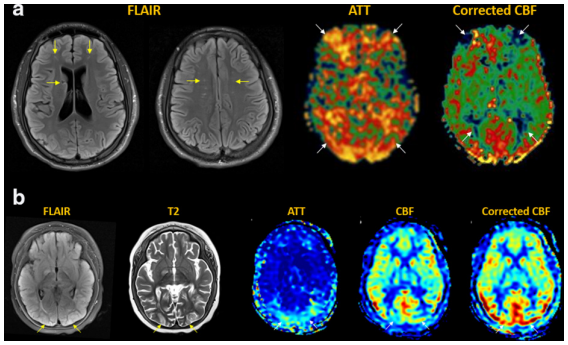

selectively vulnerable in the setting of profound HII.[73] In cases of mild or partial HII, overall decreased cerebral inflow results in watershed infarcts at the junctions of cerebral artery territories. On ASL, this manifests as the "borderzone" sign with symmetrically symmetric wedge-shaped areas of hypoperfusion along the anterior/middle and middle/posterior cerebral artery borderzones.[74,75] With severe and prolonged HII, critical and highly metabolic structures are affected including the cerebral cortex, basal ganglia, hippocampi, and cerebellum. Global anoxic injury may occur in the setting of cardiac arrest, attempted hanging, motor vehicle accidents, abusive head injury, and iatrogenic etiologies.[76–79]

MDASL is highly useful in assessing newborns and infants, who have low CBF values at baseline. Overall flow velocities may be further reduced in the setting of perinatal asphyxia and other birth complications.[28,80] In preterm infants, the cerebral circulation and neuroglial progenitor cells are immature, such that ischemic injury impacts the draining medullary veins and germinal matrix remnants. This can lead to white matter injury and intraventricular hemorrhage, respectively. In term infants, the actively developing corticospinal tracts and basal ganglia are selectively vulnerable.[81–84] Therapeutic hypothermia is the clinical standard for neuroprotection, and is intended to minimize rebound hyperperfusion leading to secondary energy failure with brain necrosis. ASL is a useful biomarker for quantifying hyperperfusion injury to vulnerable structures, and the resulting ischemic steal from other areas of brain.[84] Neonatal abstinence syndrome refers to infants with *in utero* opioid exposure from maternal drug use. At birth, infants suffer from opioid withdrawal autonomic, motor, and sensory dysregulation. MDASL perfusion metrics are elevated both globally and regionally, and correlate with abnormalities on neurologic examination.[85] [Figure 7]

Figure 7. Hypoxic-ischemic injury.(a) Watershed infarcts in patient with coagulopathy and septic shock. DWI shows bilateral external watershed infarcts (yellow arrows). MDASL shows mildly elevated ATT and decreased CBF in the external vascular borderzones (white arrows). (b) Acute anoxic injury post-cardiac arrest with diffuse cerebral edema and diffusion restriction noted throughout gray and white matter. MDASL with transit time correction shows prominent rebound hyperperfusion with diffusely elevated CBF and ACBV. (c) Preterm birth injury with Grade 3 intraventricular hemorrhage involving the bilateral caudothalamic grooves (arrows), choroid plexi, and ventricular ependyma with hydrocephalus. There is immature sulcation and patchy white matter injury with faint periventricular T2 hyperintense signal. MDASL shows decreased periventricular white matter perfusion, with more accurate estimation following transit time correction. (a) Term birth injury. ADC map shows mild diffusion restriction in the posterior limbs of internal capsules and ventrolateral thalami (yellow arrows), as well as T2 hyperintense white matter signal in the external vascular borderzones. MDASL shows elevated ATT to the external vascular borderzones (white arrows). CBF shows mild rebound hyperperfusion to the bilateral basal ganglia and corticospinal tracts (black arrows), representing areas of perinatal selective vulnerability. Transit time correction improves estimation of brain perfusion. (b) Neonatal abstinence syndrome in an infant born to an opioid-dependent mother. MDASL is useful in accurately quantifying neonatal brain perfusion, which is typically low at birth. Increased CBF at birth has been observed both globally and regionally in NAS babies relative to normal controls. Opioids alter CBF depending on baseline cerebrovascular tone, such that acute drug withdrawal likely impacts both cerebral autoregulation and autonomic activity.

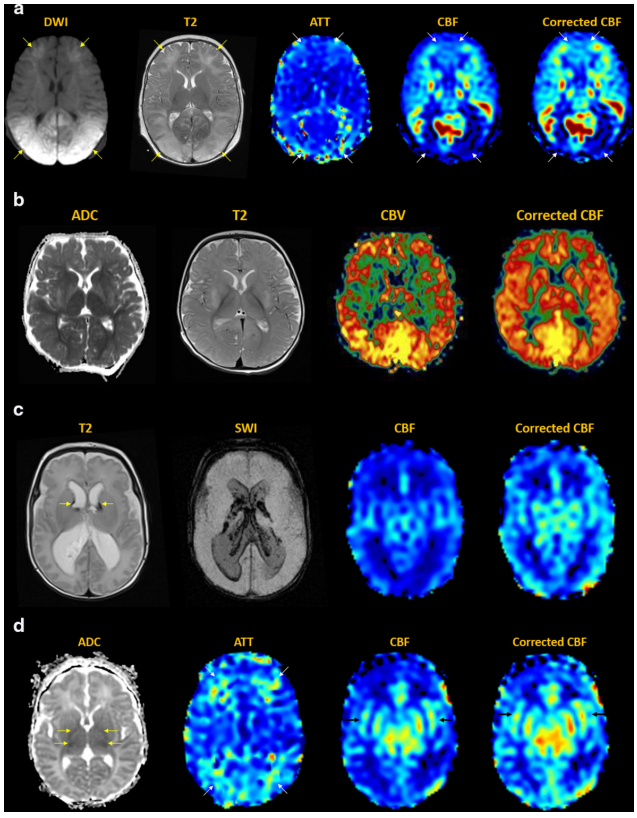

Epilepsy

Epilepsy is a complex disorder characterized by recurrent unprovoked seizures with synchronized neuronal hyperexcitability. The International League Against Epilepsy has established a framework for classification of the epilepsies. Seizures can be focal in onset, with localizing neurologic symptoms; or generalized with diffuse involvement of the brain. Etiologies are diverse and include structural, vascular, infectious, genetic, metabolic, and immune causes.[86–88] In the pediatric population, congenital brain malformations are an important diagnostic consideration. Focal cortical dysplasia (FCD) is a cause of medically refractory focal epilepsy in children that is challenging yet important to diagnose early, as appropriate intervention may enable seizure-free outcomes.[89]

Diagnostic evaluation of epilepsy consists of clinical, electrophysiologic, and imaging workup to identify the epileptogenic zone (EZ) responsible for seizure generation, which if surgically targeted leads to seizure freedom. Multimodal imaging approaches are used to lateralize and/or localize the EZ, including anatomic imaging and some combination of ASL, DSC, SPECT, and PET.[90–93] Concordance between modalities increases the likelihood of seizure-free surgical outcomes. Perfusion imaging findings in epilepsy depend on seizure pattern and timing: in focal epilepsy, the seizure focus shows hypoperfusion in the interictal period and hyperperfusion in the peri-ictal period, with statistical subtraction increasing sensitivity for EZ localization.[93] If imaging is performed after seizure onset, spreading hyperperfusion can be seen throughout the ipsilateral cerebral hemisphere. Associated limbic system connectivity can manifest with CBF increases in the ipsilateral hippocampus and thalamus (Papez circuit) and contralateral cerebellum (corticopontocerebellar pathway).[94] In patients with status epilepticus, ongoing seizure activity may yield lead to diffuse cerebral hyperperfusion with excitotoxic complications.[95,96] In patients with chronic epilepsy, MDASL can be helpful for longitudinal CBF quantification to assess treatment response (both medical and surgical). [Figure 8]

Figure 8. Epilepsy. (a) Cortical dysplasia of the right parieto-occipital region, showing disorganized sulcation with irregular gray-white junction (dotted circle). MDASL performed in interictal phase demonstrates corresponding focally decreased flow to the area of dysplasia (arrows). Because seizures are a high-flow phenomenon, transit time correction does not significantly alter the CBF results in normal brain. The area of hypoperfusion is present, though less apparent due to weighting towards longer PLDs. (b) Sturge-Weber of the left posterior quadrant with enhancing dysplastic veins in the subarachnoid space, parenchymal atrophy and gyriform calcifications (arrows). MDASL shows increased ATT and decreased CBF in the affected region (arrows). Transit time correction leads to better and more homogeneous flow quantification in normal brain. (c) Infantile spasms in West syndrome. Anatomic imaging is normal. MDASL shows diffusely elevated perfusion to cerebral cortex and basal ganglia. Findings are similar after transit time correction in this high-flow condition. (d) Chronic epilepsy in patient with Down syndrome. There is mild global volume loss and white matter signal abnormality. MDASL shows prolonged ATT and decreased CBF throughout the brain, more so along the external vascular borderzones. Transit time correction improves estimation of brain perfusion.

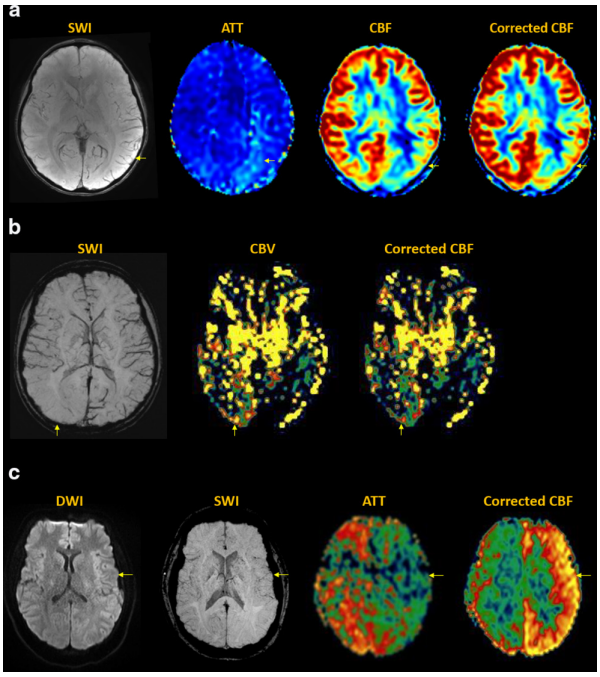

Migraine

Migraine is a neurological condition characterized by recurrent headaches and associated symptoms that can include nausea, vomiting, photophobia, phonophobia, aphasia, vision changes, and weakness or paresthesias. Migraine presents in distinct phases: prodrome (premonitory phase); aura (focal neurological deficits); headache (cephalalgic phase); and postdrome (recovery phase). There is a familial and genetic association, with hemiplegic migraine linked to mutations in ion channel and transport proteins. The theorized pathogenesis relates to cortical spreading depression with cascading effects on neural and vascular function. In patients with migraine aura, there is characteristic decreased perfusion on ASL, with accompanying vasoconstriction in some cases. Patients experience transient stroke-like symptoms corresponding to the affected brain territory. Neurologic symptoms subsequently resolve in the cephalalgic phase, with rebound vasodilation leading to headache symptoms and elevated perfusion on ASL.[97–100] Triptans are a family of serotonin receptor agonists used as abortive treatments for migraine. Therapeutic effectiveness can be monitored by ASL.[101] [Figure 9]

Trauma

Traumatic brain injury (TBI) has varying clinical manifestations depending on the mechanism, severity, and duration of injury. Anatomic imaging can be negative in mild TBI, though ASL may reveal perfusion abnormalities suggestive of occult cerebrovascular dysregulation. Low-impact injuries are associated with cerebral contusions, which tend to be greatest along the inferior frontal and anterior temporal lobes, adjacent to the rigid falx cerebri and sphenoid wings. In high-speed motor vehicle accidents, acceleration-deceleration injuries can yield diffuse axonal

Figure 9. Migraine. (a) Migraine aura. Transient right facial droop and receptive (Wernicke) aphasia. MDASL shows elevated ATT and decreased CBF to the left motor strip and posterior quadrant in a non-arterial distribution, with corresponding cortical venous engorgement (arrows). Transit time correction improves estimation of overall brain perfusion, though the hypoperfused areas are less apparent. (b) Migraine cephalalgia. Several days of right headache with left homonymous hemianopsia. MDASL with transit time correction shows rebound hyperperfusion with elevated CBF and ACBV to the right posterior quadrant, including visual cortex (arrows). There is also decreased deoxyhemoglobin content within cortical veins on SWI. (c) Therapy-resistant right hemiplegic migraine. Subtle fullness and restricted diffusion of the left cerebral cortex, with decreased cortical venous susceptibility (arrows). MDASL shows rebound hyperperfusion with decreased ATT And increased CBF throughout the left cerebral hemisphere (arrows).

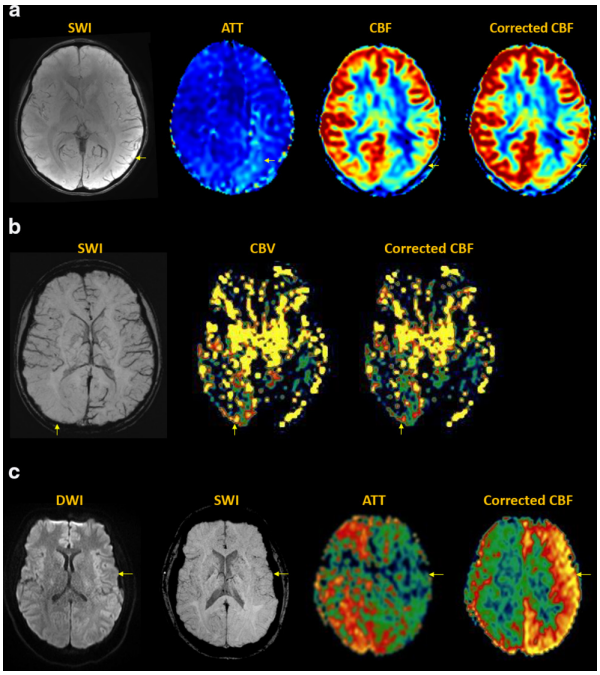

injury with shearing of the gray-white matter junction and deep structures. MDASL is helpful for quantifying cerebrovascular derangements in addition to the macrostructural findings. Multimodal advanced imaging approaches can help provide imaging biomarkers that better predict patient outcomes in TBI.[101] Abusive head trauma can also be associated with anatomic and perfusion deficits, commonly related to head-shaking and/or strangulation mechanisms.[78] [Figure 10]

Tumor

Although DSC is the clinical standard for tumor perfusion evaluation, the use of intravenous gadolinium contrast is contraindicated in certain situations—*e.g.* renal failure with risk of nephrogenic systemic fibrosis, pregnant patients in whom contrast crosses the placental barrier. Especially in children, there are concerns regarding gadolinium tissue deposition, especially when the clinical indication merits multiple follow-up MRI

Figure 10. Trauma. (a) Concussion in high school athlete with persistent language difficulties. Anatomic MRI is normal. MDASL shows heterogeneous perfusion to gray and white matter, better quantified after transit time correction. (b) Low-impact trauma from fall with bifrontal hemorrhagic cerebral contusions (arrows). MDASL shows increased ATT and decreased corrected CBF (arrows). (c) Diffuse axonal injury from motor vehicle accident with comminuted fractures, subgaleal and extraaxial hemorrhage, pontine hematoma (arrows), and diffuse cerebral edema. MDASL shows heterogeneously elevated cerebral perfusion adjacent to hemorrhage, and hypoperfusion in areas of edema. (d) Diffuse axonal injury from motor vehicle accident. Microstructural shear injury involves the gray-white junction and deep white matter (arrows). MDASL shows heterogeneously reactive cortical flow and hypoperfusion to areas of injury.

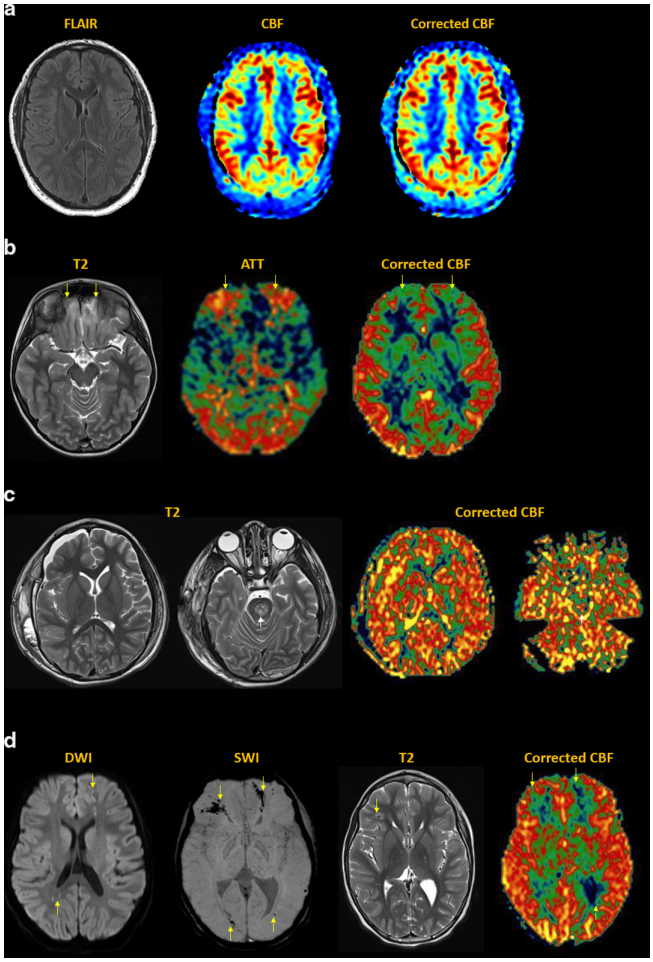

examinations. The use of MDASL provides quantitative perfusion metrics for CBF and ACBV, which correlates with tumor histology, grade, and and histopathologic vascular density in multiple studies.[102–105] ASL metrics also correlate well with DSC and other perfusion imaging modalities.[106] [Figure 11]

Infection/Inflammation

Central nervous system infection can be caused by viral, bacterial, fungal, and parasitic organisms. Potential complications include meningitis, cerebritis, brain abscess, septic thrombophlebitis,

Figure 11. Tumor. (a) Ependymoma of fourth ventricle and left foramen of Luschka, with heterogeneous internal enhancement. MDASL shows elevated CBF within tumor, more accurately quantified following transit time correction. (b) Right cerebellar pilocytic astrocytoma with solid & cystic components. MDASL shows mildly elevated CBF within solid tumor, and decreased CBF within cystic components. (c) Recurrent disseminated medulloblastoma with left frontal lobe parenchymal and leptomeningeal metastases, demonstrating enhancement and surrounding vasogenic edema (yellow arrows). MDASL shows elevated perfusion within the metastases, on a background of posttreatment encephalomalacia. Tumoral flow is better detected after transit time correction (white arrows).(d) Metastatic rhabdomyosarcoma with infiltrative cortical enhancement and vasogenic edema of left parietal lobe. MDASL shows elevated perfusion within the metastasis, and decreased perfusion in the areas of edema.

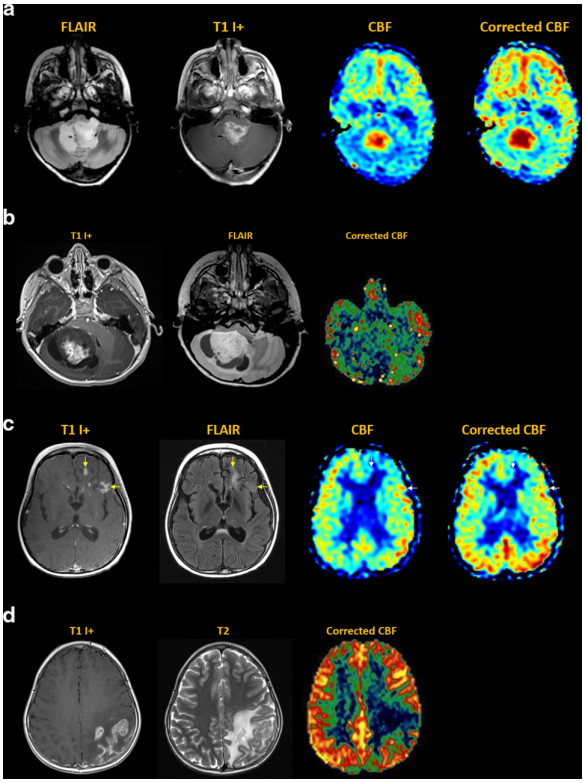

and mycotic aneurysm. ASL is helpful in assessing areas of hyperemia or ischemia due to direct parenchymal or vascular involvement.[107,108] Inflammatory and demyelinating conditions can also disrupt cerebral blood flow, presenting with hyperemia in acute disease, CBF normalization in the subacute stage, and low flow in chronic lesions.[109] [Figure 12]

Metabolic

Inherited metabolic disorders are genetic conditions that impair normal energy metabolism. Hundreds of different mechanisms exist, including failure of energy production or utilization, accumulation of toxic intermediary metabolites, and challenges with complex molecule processing and transport. Depending on the affected gene(s) and mutational severity, the clinical presentation can vary widely in terms of age and timing of onset, symptoms,

Figure 12. Infection. (a) Streptococcus pneumonia meningitis with leptomeningeal enhancement and right frontal subdural empyema (arrows). MDASL shows diffusely elevated cortical perfusion accompanying the meningeal inflammation, better estimated after transit time correction. (b) Group B streptococcus meningitis. Mild leptomeningeal enhancement with left subdural empyemas (yellow arrows). MDASL shows heterogeneously elevated flow (CBF and ACBV) along the left dura mater and cerebral cortex (white arrows).

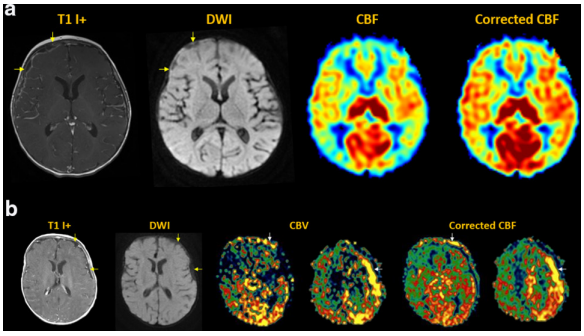

and organ systems affected. Episodes of illness or stress can precipitate or exacerbate energy decompensation.[110] ASL can be useful for distinguishing metabolic stroke-like episodes from vascular stroke. In general, metabolic crises present with one or more areas of hyperperfusion in non-vascular territories., thought to represent transient energy failure with vascular reactivity and blood-brain barrier breakdown. Perfusion abnormalities can be seen in the preclinical stage of disease and may help predict cognitive deficits.[111–115] [Figure 13]

CONCLUSIONS

MDASL is a clinically robust technique for noncontrast evaluation of cerebral blood flow. MRI labeling approaches vary by

Figure 13. Metabolic disease. (a) Batten disease with patchy white matter signal abnormality, global cerebral and cerebellar volume loss. MDASL shows prolonged ATT in the external vascular borderzones, with heterogeneous decrease in white matter CBF. (b) Nonketotic hyperglycinemia with diffuse white matter edema and restricted diffusion in bilateral corticospinal tracts (yellow arrows). MDASL with transit time correction shows elevated ACBV and CBF in the basal ganglia and corticospinal tracts (white arrows), suggesting primary energy failure. There is low perfusion to the edematous white matter.

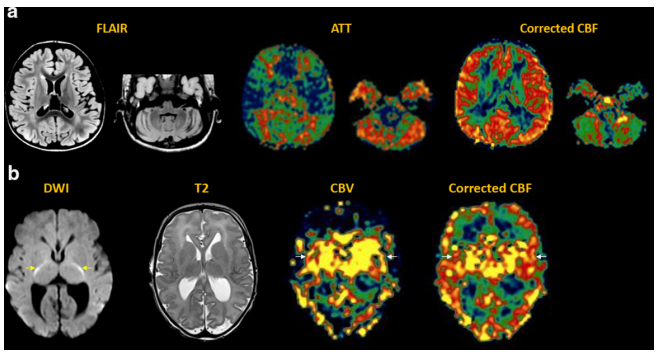

vendor and include Look-Locker, multi-TI, and Hadamard encoding approaches. Compared to single-delay ASL, MDASL enables more accurate and reproducible quantification of CBF and other perfusion parameters, such as ATT and ACBV. Due to practical limitations in imaging time and SNR, as well as potential overestimation with simpler models, MDASL is most helpful in young subjects and slow-flow conditions. We review major clinical applications in the pediatric brain including stroke, vasculopathy, hypoxic-ischemic injury, epilepsy, migraine, tumor, infection, and metabolic disease.

ACKNOWLEDGMENT

M.L.H. received the Magna Cum Laude Award at the American Society of Neuroradiology 2021 meeting for an educational exhibit on this topic.

CONFLICTS OF INTEREST

X.G. is supported by the National Institute for Health Research University College London Hospitals Biomedical Research Centre. M.L.H. is funded by NIBIB R01 EB029957, NIH R01 NS 041922, DOD Exploration-Hypothesis Development Award TS200051, and Italfarmaco: principal investigator on completed grants including Siemens Healthineers / Radiological Society of North America Research Scholar Grant, Society for Pediatric Radiology Pilot Award, and American Society of Head and Neck Radiology William N. Hanafee Grant; and co-investigator on the Bayer Healthcare Radiology Medical Education Grant and CHEST Foundation Research Grant in Cystic Fibrosis, for work unrelated to this article

REFERENCES

1. Detre JA, Leigh JS, Williams DS, Koretsky AP. Perfusion imaging. *Magn Reson Med* 1992; **23**: 37–45. https://doi.org/10.1002/mrm.1910230106
2. Williams DS, Detre JA, Leigh JS, Koretsky AP. Magnetic resonance imaging of perfusion using spin inversion of arterial water. [Internet]. *Proc Natl Acad Sci U S A* 1992; **89**: 212–16. https://doi.org/10.1073/pnas.89.1.212
3. Alsop DC, Detre JA, Golay X, Günther M, Hendrikse J, Hernandez-Garcia L, et al. Recommended implementation of arterial spin-labeled perfusion MRI for clinical applications: A consensus of the ISMRM perfusion study group and the european consortium for ASL in dementia. *Magn Reson Med* 2015; **73**: 102–16. https://doi.org/10.1002/mrm.25197
4. Kim SG. Quantification of relative cerebral blood flow change by flow-sensitive alternating inversion recovery (FAIR) technique: application to functional mapping. *Magn Reson Med* 1995; **34**: 293–301. https://doi.org/10.1002/mrm.1910340303
5. Edelman RR, Chen Q. EPISTAR MRI: multislice mapping of cerebral blood flow. *Magn Reson Med* 1998; **40**: 800–805. https://doi.org/10.1002/mrm.1910400603
6. Wong EC, Buxton RB, Frank LR. Quantitative imaging of perfusion using a single subtraction (QUIPSS and QUIPSS ii). *Magn Reson Med* 1998; **39**: 702–8. https://doi.org/10.1002/mrm.1910390506
7. Dai W, Garcia D, BC, Alsop DC. Continuous flow-driven inversion for arterial spin labeling using pulsed radio frequency and gradient fields. *Magn Reson Med* 2008; **60**: 1488–97. https://doi.org/10.1002/mrm.21790
8. Wong EC, Cronin M, Wu WC, Inglis B, Frank LR, Liu TT. Velocity-selective arterial spin labeling. *Magn Reson Med* 2006; **55**: 1334–41. https://doi.org/10.1002/mrm.20906
9. Alsop DC, Detre JA. Reduced transit-time sensitivity in noninvasive magnetic resonance imaging of human cerebral blood flow. *J Cereb Blood Flow Metab* 1996; **16**: 1236–49. https://doi.org/10.1097/00004647-199611000-00019
10. Bokkers RPH, van der Worp HB, Mali WPTM, Hendrikse J. Noninvasive MR imaging of cerebral perfusion in patients with a carotid artery stenosis. *Neurology* 2009; **73**: 869–75. https://doi.org/10.1212/WNL.0b013e3181b7840c
11. Hendrikse J, Lu H, van der Grond J, Van Zijl PCM, Golay X. Measurements of cerebral perfusion and arterial hemodynamics during visual stimulation using turbo-TILT. *Magn Reson Med* 2003; **50**: 429–33. https://doi.org/10.1002/mrm.10525
12. Günther M, Bock M, Schad LR. Arterial spin labeling in combination with a look-locker sampling strategy: inflow turbo-sampling EPI-FAIR (ITS-FAIR). *Magn Reson Med* 2001; **46**: 974–84. https://doi.org/10.1002/mrm.1284
13. Petersen ET, Lim T, Golay X. Model-free arterial spin labeling quantification approach for perfusion MRI. *Magn Reson Med* 2006; **55**: 219–32. https://doi.org/10.1002/mrm.20784
14. von Samson-Himmelstjerna F, Madai VI, Sobesky J, Guenther M. Walsh-ordered hadamard time-encoded pseudocontinuous ASL (WH pcasl). *Magn Reson Med* 2016; **76**: 1814–24. https://doi.org/10.1002/mrm.26078
15. MacIntosh BJ, Filippini N, Chappell MA, Woolrich MW, Mackay CE, Jezzard P. Assessment of arterial arrival times derived from multiple inversion time pulsed arterial spin labeling MRI. *Magn Reson Med* 2010; **63**: 641–47. https://doi.org/10.1002/mrm.22256
16. Günther M, Oshio K, Feinberg DA. Single-shot 3D imaging techniques improve arterial spin labeling perfusion measurements. *Magn Reson Med* 2005; **54**: 491–98. https://doi.org/10.1002/mrm.20580
17. Chappell MA, MacIntosh BJ, Donahue MJ, Günther M, Jezzard P, Woolrich MW. Separation of macrovascular signal in multi-inversion time arterial spin labelling MRI. *Magn Reson Med* 2010; **63**: 1357–65. https://doi.org/10.1002/mrm.22320
18. Buxton RB, Frank LR, Wong EC, Siewert B, Warach S, Edelman RR. A general kinetic model for quantitative perfusion imaging with arterial spin labeling. *Magn Reson Med* 1998; **40**: 383–96. https://doi.org/10.1002/mrm.1910400308
19. Østergaard L. Principles of cerebral perfusion imaging by bolus tracking. *J Magn Reson Imaging* 2005; **22**: 710–17. https://doi.org/10.1002/jmri.20460
20. Guo J, Holdsworth SJ, Fan AP, Lebel MR, Zun Z, Shankaranarayanan A, et al. Comparing accuracy and reproducibility of sequential and hadamard-encoded multidelay pseudocontinuous arterial spin labeling for measuring cerebral blood flow and arterial transit time in healthy subjects: A simulation and in vivo study. *J Magn Reson Imaging* 2018; **47**: 1119–32. https://doi.org/10.1002/jmri.25834
21. Gevers S, van Osch MJ, Bokkers RPH, Kies DA, Teeuwisse WM, Majoie CB, et al.

Intra- and multicenter reproducibility of pulsed, continuous and pseudo-continuous arterial spin labeling methods for measuring cerebral perfusion. *J Cereb Blood Flow Metab* 2011; **31**: 1706–15. https://doi.org/10.1038/jcbfm.2011.10
22. Lin T, Qu J, Zuo Z, Fan X, You H, Feng F. Test-retest reliability and reproducibility of long-label pseudo-continuous arterial spin labeling. *Magn Reson Imaging* 2020; **73**: S0730-725X(20)30092-8: 111–17: . https://doi.org/10.1016/j.mri.2020.07.010
23. Qin Q, Huang AJ, Hua J, Desmond JE, Stevens RD, van Zijl PCM. Three-dimensional whole-brain perfusion quantification using pseudo-continuous arterial spin labeling MRI at multiple post-labeling delays: accounting for both arterial transit time and impulse response function. *NMR Biomed* 2014; **27**: 116–28. https://doi.org/10.1002/nbm.3040
24. Martin SZ, Madai VI, von Samson-Himmelstjerna FC, Mutke MA, Bauer M, Herzig CX, et al. 3D GRASE pulsed arterial spin labeling at multiple inflow times in patients with long arterial transit times: comparison with dynamic susceptibility-weighted contrast-enhanced MRI at 3 tesla. *J Cereb Blood Flow Metab* 2015; **35**: 392–401. https://doi.org/10.1038/jcbfm.2014.200
25. Sugimori H, Fujima N, Suzuki Y, Hamaguchi H, Sakata M, Kudo K. Evaluation of cerebral blood flow using multi-phase pseudo continuous arterial spin labeling at 3-tesla. *Magn Reson Imaging* 2015; **33**: S0730-725X(15)00192-7: 1338–44: . https://doi.org/10.1016/j.mri.2015.07.016
26. Johnston ME, Lu K, Maldjian JA, Jung Y. Multi-TI arterial spin labeling MRI with variable TR and bolus duration for cerebral blood flow and arterial transit time mapping. *IEEE Trans Med Imaging* 2015; **34**: 1392–1402. https://doi.org/10.1109/TMI.2015.2395257
27. Yun TJ, Sohn CH, Yoo RE, Kang KM, Choi SH, Kim JH, et al. Transit time corrected arterial spin labeling technique aids to overcome delayed transit time effect. *Neuroradiology* 2018; **60**: 255–65. https://doi.org/10.1007/s00234-017-1969-x
28. Kim HG, Lee JH, Choi JW, Han M, Gho SM, Moon Y. Multidelay arterial spin-labeling MRI in neonates and infants: cerebral perfusion changes during brain maturation. *AJNR Am J Neuroradiol* 2018; **39**: 1912–18. https://doi.org/10.3174/ajnr.A5774
29. Zaharchuk G. Arterial transit awesomeness. *Radiology* 2020; **297**: 661–62. https://doi.org/10.1148/radiol.2020203838
30. Jaganmohan D, Pan S, Kesavadas C, Thomas B. A pictorial review of brain arterial spin labelling artefacts and their potential remedies in clinical studies. *Neuroradiol J* 2021; **34**: 154–68. https://doi.org/10.1177/1971400920977031
31. Deibler AR, Pollock JM, Kraft RA, Tan H, Burdette JH, Maldjian JA. Arterial spin-labeling in routine clinical practice, part 1: technique and artifacts. *AJNR Am J Neuroradiol* 2008; **29**: 1228–34. https://doi.org/10.3174/ajnr.A1030
32. . Amukotuwa SA, Yu C, Zaharchuk G. 3D Pseudocontinuous arterial spin labeling in routine clinical practice: A review of clinically significant artifacts. J Magn Reson Imaging 2016;43(1):11-27.
33. Bladt P, van Osch MJP, Clement P, Achten E, Sijbers J, den Dekker AJ. Supporting measurements or more averages? how to quantify cerebral blood flow most reliably in 5 minutes by arterial spin labeling. *Magn Reson Med* 2020; **84**: 2523–36. https://doi.org/10.1002/mrm.28314
34. Maier O, Spann SM, Pinter D, Gattringer T, Hinteregger N, Thallinger GG, et al. Non-linear fitting with joint spatial regularization in arterial spin labeling. *Medical Image Analysis* 2021; **71**: 102067. https://doi.org/10.1016/j.media.2021.102067
35. Madai VI, Martin SZ, von Samson-Himmelstjerna FC, Herzig CX, Mutke MA, Wood CN, et al. Correction for susceptibility distortions increases the performance of arterial spin labeling in patients with cerebrovascular disease. *J Neuroimaging* 2016; **26**: 436–44. https://doi.org/10.1111/jon.12331
36. Petr J, Schramm G, Hofheinz F, Langner J, van den Hoff J. Modeling magnetization transfer effects of Q2TIPS bolus saturation in multi-TI pulsed arterial spin labeling. *Magn Reson Med* 2014; **72**: 1007–14. https://doi.org/10.1002/mrm.25011
37. Zhang LX, Woods JG, Okell TW, Chappell MA. Examination of optimized protocols for pcasl: sensitivity to macrovascular contamination, flow dispersion, and prolonged arterial transit time. *Magn Reson Med* 2021; **86**: 2208–19. https://doi.org/10.1002/mrm.28839
38. Kramme J, Gregori J, Diehl V, Madai VI, von Samson-Himmelstjerna FC, Lentschig M, et al. Improving perfusion quantification in arterial spin labeling for delayed arrival times by using optimized acquisition schemes. *Z Med Phys* 2015; **25**: S0939-3889(14)00094-4: 221–29: . https://doi.org/10.1016/j.zemedi.2014.07.003
39. Paschoal AM, Leoni RF, Foerster BU, Dos Santos AC, Pontes-Neto OM, Paiva FF. Contrast optimization in arterial spin labeling with multiple post-labeling delays for cerebrovascular assessment. *MAGMA* 2021; **34**: 119–31. https://doi.org/10.1007/s10334-020-00883-z
40. Woods JG, Chappell MA, Okell TW. Designing and comparing optimized pseudo-continuous arterial spin labeling protocols for measurement of cerebral blood flow. *Neuroimage* 2020; **223**: : S1053-8119(20)30732-1. https://doi.org/10.1016/j.neuroimage.2020.117246
41. Woods JG, Chappell MA, Okell TW. A general framework for optimizing arterial spin labeling MRI experiments. *Magn Reson Med* 2019; **81**: 2474–88. https://doi.org/10.1002/mrm.27580
42. Zaharchuk G. Arterial spin label imaging of acute ischemic stroke and transient ischemic attack. *Neuroimaging Clin N Am* 2011; **21**: 285–301, . https://doi.org/10.1016/j.nic.2011.01.003
43. Guo L, Zhang Q, Ding L, Liu K, Ding K, Jiang C, et al. Pseudo-continuous arterial spin labeling quantifies cerebral blood flow in patients with acute ischemic stroke and chronic lacunar stroke. *Clin Neurol Neurosurg* 2014; **125**: S0303-8467(14)00323-0: 229–36: . https://doi.org/10.1016/j.clineuro.2014.08.017
44. Chen J, Zhao B, Bu C, Xie G. Relationship between the hemodynamic changes on multi-td pulsed arterial spin labeling images and the degrees of cerebral artery stenosis. *Magn Reson Imaging* 2014; **32**: S0730-725X(14)00248-3: 1277–83: . https://doi.org/10.1016/j.mri.2014.08.017
45. Amemiya S, Watanabe Y, Takei N, Ueyama T, Miyawaki S, Koizumi S, et al. Arterial transit time-based multidelay combination strategy improves arterial spin labeling cerebral blood flow measurement accuracy in severe steno-occlusive diseases. *J Magn Reson Imaging* 2022; **55**: 178–87. https://doi.org/10.1002/jmri.27823
46. Wolf ME, Layer V, Gregori J, Griebe M, Szabo K, Gass A, et al. Assessment of perfusion deficits in ischemic stroke using 3D-GRASE arterial spin labeling magnetic resonance imaging with multiple inflow times. *J Neuroimaging* 2014; **24**: 453–59. https://doi.org/10.1111/jon.12064
47. Lou X, Yu S, Scalzo F, Starkman S, Ali LK, Kim D, et al. Multi-delay ASL can identify leptomeningeal collateral perfusion in endovascular therapy of ischemic stroke. *Oncotarget* 2017; **8**: 2437–43. https://doi.org/10.18632/oncotarget.13898
48. Wang DJJ, Alger JR, Qiao JX, Gunther M, Pope WB, Saver JL, et al. Multi-delay multi-parametric arterial spin-labeled perfusion MRI in acute ischemic stroke - comparison with dynamic susceptibility contrast

enhanced perfusion imaging. *Neuroimage Clin* 2013; **3**: 1–7. https://doi.org/10.1016/j.nicl.2013.06.017
49. Xu X, Tan Z, Fan M, Ma M, Fang W, Liang J, et al. Comparative study of multi-delay pseudo-continuous arterial spin labeling perfusion MRI and CT perfusion in ischemic stroke disease. *Front Neuroinform* 2021; **15**: 719719. https://doi.org/10.3389/fninf.2021.719719
50. Amemiya S, Takao H, Watanabe Y, Takei N, Ueyama T, Kato S, et al. Reliability and sensitivity to longitudinal CBF changes in steno-occlusive diseases: ASL versus ^{123}I-imp-SPECT. *J Magn Reson Imaging* 2021. https://doi.org/10.1002/jmri.27996
51. Hendrikse J, Petersen ET, Golay X. Vascular disorders: insights from arterial spin labeling. *Neuroimaging Clin N Am* 2012; **22**: 259–69, . https://doi.org/10.1016/j.nic.2012.02.003
52. Kang JH, Yun TJ, Yoo RE, Yoon BW, Lee AL, Kang KM, et al. Bright sinus appearance on arterial spin labeling MR imaging aids to identify cerebral venous thrombosis. *Medicine (Baltimore)* 2017; **96**(41): e8244. https://doi.org/10.1097/MD.0000000000008244
53. Furuya S, Kawabori M, Fujima N, Tokairin K, Goto S, Iwasaki M, et al. Serial arterial spin labeling may be useful in assessing the therapeutic course of cerebral venous thrombosis: case reports. *Neurol Med Chir (Tokyo)* 2017; **57**: 557–61. https://doi.org/10.2176/nmc.cr.2017-0033
54. Kronenburg A, Bulder MMM, Bokkers RPH, Hartkamp NS, Hendrikse J, Vonken E-J, et al. Cerebrovascular reactivity measured with ASL perfusion MRI, ivy sign, and regional tissue vascularization in moyamoya. *World Neurosurg* 2019; **125**: S1878-8750(19)30240-2: e639–50: . https://doi.org/10.1016/j.wneu.2019.01.140
55. Zaharchuk G, Do HM, Marks MP, Rosenberg J, Moseley ME, Steinberg GK. Arterial spin-labeling MRI can identify the presence and intensity of collateral perfusion in patients with moyamoya disease. *Stroke* 2011; **42**: 2485–91. https://doi.org/10.1161/STROKEAHA.111.616466
56. Ha JY, Choi YH, Lee S, Cho YJ, Cheon JE, Kim IO, et al. Arterial spin labeling MRI for quantitative assessment of cerebral perfusion before and after cerebral revascularization in children with moyamoya disease. *Korean J Radiol* 2019; 985–96.
57. Ni WW, Christen T, Rosenberg J, Zun Z, Moseley ME, Zaharchuk G. Imaging of cerebrovascular reserve and oxygenation in moyamoya disease. *J Cereb Blood Flow Metab* 2017; 1213–22. https://doi.org/10.1177/0271678X16651088
58. Federau C, Christensen S, Zun Z, Park SW, Ni W, Moseley M, et al. Cerebral blood flow, transit time, and apparent diffusion coefficient in moyamoya disease before and after acetazolamide. *Neuroradiology* 2017; 5–12.
59. Wang R, Yu S, Alger JR, Zuo Z, Chen J, Wang R, et al. Multi-delay arterial spin labeling perfusion MRI in moyamoya disease--comparison with CT perfusion imaging. *Eur Radiol* 2014; **24**: 1135–44. https://doi.org/10.1007/s00330-014-3098-9
60. Qiu D, Straka M, Zun Z, Bammer R, Moseley ME, Zaharchuk G. CBF measurements using multidelay pseudocontinuous and velocity-selective arterial spin labeling in patients with long arterial transit delays: comparison with xenon CT CBF. *J Magn Reson Imaging* 2012; 110–19.
61. Fan AP, Guo J, Khalighi MM, Gulaka PK, Shen B, Park JH, et al. Long-delay arterial spin labeling provides more accurate cerebral blood flow measurements in moyamoya patients: A simultaneous positron emission tomography/MRI study. *Stroke* 2017; **48**: 2441–49. https://doi.org/10.1161/STROKEAHA.117.017773
62. Fan AP, Khalighi MM, Guo J, Ishii Y, Rosenberg J, Wardak M, et al. Identifying hypoperfusion in moyamoya disease with arterial spin labeling and an [^{15} o]-water positron emission tomography/magnetic resonance imaging normative database . *Stroke* 2019; **50**: 373–80. https://doi.org/10.1161/STROKEAHA.118.023426
63. Zhao MY, Fan AP, Chen DY-T, Sokolska MJ, Guo J, Ishii Y, et al. Cerebrovascular reactivity measurements using simultaneous ^{15}o-water PET and ASL MRI: impacts of arterial transit time, labeling efficiency, and hematocrit. *Neuroimage* 2021; **233**: S1053-8119(21)00232-9. https://doi.org/10.1016/j.neuroimage.2021.117955
64. Bulder MMM, Bokkers RPH, Hendrikse J, Kappelle LJ, Braun KPJ, Klijn CJM. Arterial spin labeling perfusion MRI in children and young adults with previous ischemic stroke and unilateral intracranial arteriopathy. *Cerebrovasc Dis* 2014; **37**: 14–21. https://doi.org/10.1159/000355889
65. Juttukonda MR. Donahue MJ1,2,3,4, davis LT1, gindville MC5, lee CA5, patel NJ5, kassim AA6, pruthi S1, hendrikse J7, jordan LC2,5. preliminary evidence for cerebral capillary shunting in adults with sickle cell anemia. *J Cereb Blood Flow Metab* 2019; **39**: 1099–1110.
66. Juttukonda MR, Jordan LC, Gindville MC, Davis LT, Watchmaker JM, Pruthi S, et al. Cerebral hemodynamics and pseudo-continuous arterial spin labeling considerations in adults with sickle cell anemia. *NMR Biomed* 2017; **30**(2). https://doi.org/10.1002/nbm.3681
67. Shen Y, Zhao B, Yan L, Jann K, Wang G, Wang J, et al. Cerebral hemodynamic and white matter changes of type 2 diabetes revealed by multi-TI arterial spin labeling and double inversion recovery sequence. *Front Neurol* 2017; **8**: 717. https://doi.org/10.3389/fneur.2017.00717
68. Jia J, Xie J, Li H, Wei H, Li X, Hu J, et al. Cerebral blood flow abnormalities in neuropsychiatric systemic lupus erythematosus. *Lupus* 2019; **28**: 1128–33. https://doi.org/10.1177/0961203319861677
69. Zhuo Z, Su L, Duan Y, Huang J, Qiu X, Haller S, et al. Different patterns of cerebral perfusion in SLE patients with and without neuropsychiatric manifestations. *Hum Brain Mapp* 2020; **41**: 755–66. https://doi.org/10.1002/hbm.24837
70. Hoogeveen ES, Pelzer N, Ghariq E, van Osch MJ, Dahan A, Terwindt GM, et al. Cerebrovascular reactivity in retinal vasculopathy with cerebral leukoencephalopathy and systemic manifestations. *J Cereb Blood Flow Metab* 2021; **41**: 831–40. https://doi.org/10.1177/0271678X20929430
71. Kayfan S, Sharifi A, Xie S, Yin C, Pfeifer CM. MRA and ASL perfusion findings in pediatric reversible cerebral vasoconstriction syndrome. *Radiol Case Rep* 2019; **14**: 832–36. https://doi.org/10.1016/j.radcr.2019.04.010
72. Wakisaka K, Morioka T, Shimogawa T, Murao K, Kanazawa Y, Hagiwara N, et al. Epileptic ictal hyperperfusion on arterial spin labeling perfusion and diffusion-weighted magnetic resonance images in posterior reversible encephalopathy syndrome. *J Stroke Cerebrovasc Dis* 2016; **25**: S1052-3057(15)00509-1: 228–37: . https://doi.org/10.1016/j.jstrokecerebrovasdis.2015.09.023
73. Huang BY, Castillo M. Hypoxic-ischemic brain injury: imaging findings from birth to adulthood. *Radiographics* 2008; **28**: 417–39; . https://doi.org/10.1148/rg.282075066
74. Mangla R, Kolar B, Almast J, Ekholm SE. Border zone infarcts: pathophysiologic and imaging characteristics. *Radiographics* 2011; **31**: 1201–14. https://doi.org/10.1148/rg.315105014
75. Zaharchuk G, Bammer R, Straka M, Shankaranarayan A, Alsop DC, Fischbein NJ, et al. Arterial spin-label imaging in

patients with normal bolus perfusion-weighted MR imaging findings: pilot identification of the borderzone sign. *Radiology* 2009; **252**: 797–807. https://doi.org/10.1148/radiol.2523082018
76. Iordanova B1, li L2, clark RSB3,4, manole MD3. alterations in cerebral blood flow after resuscitation from cardiac arrest. *Front Pediatr* 2017; **5**: 174. https://doi.org/10.3389/fped.2017.00174
77. Li N, Wingfield MA, Nickerson JP, Pettersson DR, Pollock JM. Anoxic brain injury detection with the normalized diffusion to ASL perfusion ratio: implications for blood-brain barrier injury and permeability. *AJNR Am J Neuroradiol* 2020; **41**: 598–606. https://doi.org/10.3174/ajnr.A6461
78. Wong AM-C, Yeh C-H, Liu H-L, Wu T-W, Lin K-L, Wang H-S, et al. Arterial spin-labeling perfusion imaging of children with subdural hemorrhage: perfusion abnormalities in abusive head trauma. *J Neuroradiol* 2017; **44**: S0150-9861(16)30135-3: 281–87: . https://doi.org/10.1016/j.neurad.2017.02.003
79. Prosser DD, Grigsby T, Pollock JM. Unilateral anoxic brain injury secondary to strangulation identified on conventional and arterial spin-labeled perfusion imaging. *Radiol Case Rep* 2018; **13**: 563–67. https://doi.org/10.1016/j.radcr.2018.02.004
80. Tortora D, Severino M, Rossi A. Arterial spin labeling perfusion in neonates. *Semin Fetal Neonatal Med* 2020; **25**: S1744-165X(20)30055-X: 101130: . https://doi.org/10.1016/j.siny.2020.101130
81. Kim HG, Choi JW, Lee JH, Jung DE, Gho SM. Association of cerebral blood flow and brain tissue relaxation time with neurodevelopmental outcomes of preterm neonates: multidelay arterial spin labeling and synthetic MRI study. *Invest Radiol* 2022; **57**: 254–62. https://doi.org/10.1097/RLI.0000000000000833
82. Bouyssi-Kobar M, Murnick J, Brossard-Racine M, Chang T, Mahdi E, Jacobs M, et al. Altered cerebral perfusion in infants born preterm compared with infants born full term. *J Pediatr* 2018; **193**: S0022-3476(17)31338-0: 54-61. . https://doi.org/10.1016/j.jpeds.2017.09.083
83. Miranda MJ, Olofsson K, Sidaros K. Noninvasive measurements of regional cerebral perfusion in preterm and term neonates by magnetic resonance arterial spin labeling. *Pediatr Res* 2006; **60**: 359–63. https://doi.org/10.1203/01.pdr.0000232785.00965.b3
84. Watson CG, Dehaes M, Gagoski BA, Grant PE, Rivkin MJ. Arterial spin labeling perfusion magnetic resonance imaging performed in acute perinatal stroke reveals hyperperfusion associated with ischemic injury. *Stroke* 2016; **47**: 1514–19. https://doi.org/10.1161/STROKEAHA.115.011936
85. Benninger KL, Peng J, Ho ML, Newton J, Wang DJJ, Hu HH, et al. Cerebral perfusion and neurological examination characterise neonatal opioid withdrawal syndrome: a prospective cohort study. *Arch Dis Child Fetal Neonatal Ed* 2021: fetalneonatal-2021-322192. https://doi.org/10.1136/archdischild-2021-322192
86. Scheffer IE, Berkovic S, Capovilla G, Connolly MB, French J, Guilhoto L, et al. ILAE classification of the epilepsies: position paper of the ILAE commission for classification and terminology. *Epilepsia* 2017; **58**: 512–21. https://doi.org/10.1111/epi.13709
87. Fisher RS, Cross JH, French JA, Higurashi N, Hirsch E, Jansen FE, et al. Operational classification of seizure types by the international league against epilepsy: position paper of the ILAE commission for classification and terminology. *Epilepsia* 2017; **58**: 522–30. https://doi.org/10.1111/epi.13670
88. Pressler RM, Cilio MR, Mizrahi EM, Moshé SL, Nunes ML, Plouin P, et al. (n.d.). The ILAE classification of seizures and the epilepsies: modification for seizures in the neonate. *Position Paper by the ILAE Task Force on Neonatal Seizures Epilepsia*; **62**: 615–28. https://doi.org/10.1111/epi.16815
89. Blauwblomme T, Boddaert N, Chémaly N, Chiron C, Pages M, Varlet P, et al. Arterial spin labeling MRI: a step forward in non-invasive delineation of focal cortical dysplasia in children. *Epilepsy Res* 2014; **108**: S0920-1211(14)00272-1: 1932–39: . https://doi.org/10.1016/j.eplepsyres.2014.09.029
90. Zeng JY, Hu XQ, Xu JF, Zhu WJ, Wu HY, Dong FJ. Diagnostic accuracy of arterial spin-labeling MR imaging in detecting the epileptogenic zone: systematic review and meta-analysis. *AJNR Am J Neuroradiol* 2021; **42**: 1052–60. https://doi.org/10.3174/ajnr.A7061
91. Nagesh C1, kumar S1, menon R2, thomas B1, radhakrishnan A2, kesavadas C1. the imaging of localization related symptomatic epilepsies: the value of arterial spin labelling based magnetic resonance perfusion. *Korean J Radiol* 2018; 965–77. https://doi.org/10.3348/kjr.2018.19.5.965
92. Oner AY, Eryurt B, Ucar M, Capraz I, Kurt G, Bilir E, et al. PASL versus DSC perfusion MRI in lateralizing temporal lobe epilepsy. *Acta Radiol* 2015; **56**: 477–81. https://doi.org/10.1177/0284185114531128
93. Pizzini FB, Farace P, Manganotti P, Zoccatelli G, Bongiovanni LG, Golay X, et al. Cerebral perfusion alterations in epileptic patients during peri-ictal and post-ictal phase: PASL vs DSC-MRI. *Magn Reson Imaging* 2013; **31**: S0730-725X(13)00109-4: 1001–5: . https://doi.org/10.1016/j.mri.2013.03.023
94. Takane Y, Shibata K, Nishimura Y, Sakura H. Crossed cerebellar and contralateral thalamic hyperperfusion in epilepsy. *Intern Med* 2017; **56**: 1121–22. https://doi.org/10.2169/internalmedicine.56.7632
95. Chen G, Lei D, Ren J, Zuo P, Suo X, Wang DJJ, et al. Patterns of postictal cerebral perfusion in idiopathic generalized epilepsy: a multi-delay multi-parametric arterial spin labelling perfusion MRI study. *Sci Rep* 2016; **6**(1). https://doi.org/10.1038/srep28867
96. Kim TJ, Choi JW, Han M, Kim BG, Park SA, Huh K, et al. Usefulness of arterial spin labeling perfusion as an initial evaluation of status epilepticus. *Sci Rep* 2021; **11**(1): 24218. https://doi.org/10.1038/s41598-021-03698-7
97. Cadiot D, Longuet R, Bruneau B, Treguier C, Carsin-Vu A, Corouge I, et al. Magnetic resonance imaging in children presenting migraine with aura: association of hypoperfusion detected by arterial spin labelling and vasospasm on MR angiography findings. *Cephalalgia* 2018; **38**: 949–58. https://doi.org/10.1177/0333102417723570
98. Cobb-Pitstick KM, Munjal N, Safier R, Cummings DD, Zuccoli G. Time course of cerebral perfusion changes in children with migraine with aura mimicking stroke. *AJNR Am J Neuroradiol* 2018; **39**: 1751–55. https://doi.org/10.3174/ajnr.A5693
99. Wolf ME, Okazaki S, Eisele P, Rossmanith C, Gregori J, Griebe M, et al. Arterial spin labeling cerebral perfusion magnetic resonance imaging in migraine aura: an observational study. *J Stroke Cerebrovasc Dis* 2018; **27**: S1052-3057(17)30664-X: 1262–66: . https://doi.org/10.1016/j.jstrokecerebrovasdis.2017.12.002
100. Kato Y, Araki N, Matsuda H, Ito Y, Suzuki C. Arterial spin-labeled MRI study of migraine attacks treated with rizatriptan. *J Headache Pain* 2010; **11**: 255–58. https://doi.org/10.1007/s10194-010-0215-2
101. Andre JB. Arterial spin labeling magnetic resonance perfusion for traumatic brain injury: technical challenges and potentials. *Top Magn Reson Imaging* 2015; **24**: 275–87. https://doi.org/10.1097/RMR.0000000000000065

102. Kikuchi K, Hiwatashi A, Togao O, Yamashita K, Yoshimoto K, Mizoguchi M, et al. Correlation between arterial spin-labeling perfusion and histopathological vascular density of pediatric intracranial tumors. *J Neurooncol* 2017; **135**: 561–69. https://doi.org/10.1007/s11060-017-2604-8
103. Delgado AF, De Luca F, Hanagandi P, van Westen D, Delgado AF. Arterial spin-labeling in children with brain tumor: A meta-analysis. *AJNR Am J Neuroradiol* 2018; **39**: 1536–42. https://doi.org/10.3174/ajnr.A5727
104. Vidyasagar R, Abernethy L, Pizer B, Avula S, Parkes LM. Quantitative measurement of blood flow in paediatric brain tumours-a comparative study of dynamic susceptibility contrast and multi time-point arterial spin labelled MRI. *Br J Radiol* 2016; **89**(1062): 20150624. https://doi.org/10.1259/bjr.20150624
105. Yang S, Zhao B, Wang G, Xiang J, Xu S, Liu Y, et al. Improving the grading accuracy of astrocytic neoplasms noninvasively by combining timing information with cerebral blood flow: A multi-TI arterial spin-labeling MR imaging study. *AJNR Am J Neuroradiol* 2016; **37**: 2209–16. https://doi.org/10.3174/ajnr.A4907
106. Maral H, Ertekin E, Tunçyürek Ö, Özsunar Y. Effects of susceptibility artifacts on perfusion MRI in patients with primary brain tumor: A comparison of arterial spin-labeling versus DSC. *AJNR Am J Neuroradiol* 2020; **41**: 255–61. https://doi.org/10.3174/ajnr.A6384
107. Noguchi T, Yakushiji Y, Nishihara M, Togao O, Yamashita K, Kikuchi K, et al. Arterial spin-labeling in central nervous system infection. *Magn Reson Med Sci* 2016; **15**: 386–94. https://doi.org/10.2463/mrms.mp.2015-0140
108. Kumar S, Gutch M. Advanced magnetic resonance imaging techniques in tuberculous meningitis. *Adv Biomed Res* 2020; **9**: 20. https://doi.org/10.4103/abr.abr_222_19
109. Zhang X. Guo X1, zhang N1, cai H2, sun J1, wang Q1, qi Y3, zhang L3, yang L3, shi FD3, yu C1. cerebral blood flow changes in multiple sclerosis and neuromyelitis optica and their correlations with clinical disability. *Front Neurol* 2018. https://doi.org/10.3389/fneur.2018.00305
110. Ferreira CR, Rahman S, Keller M, Zschocke J, Group IA. An international classification of inherited metabolic disorders (ICIMD). *J Inherit Metab Dis* 2021; **44**: 164–77. https://doi.org/10.1002/jimd.12348
111. Li X, Wang Y, Wang Z, Lu J, Xu Y, Ye J, et al. Comparison of magnetic resonance spectroscopy (MRS) with arterial spin labeling (ASL) in the differentiation between mitochondrial encephalomyopathy, lactic acidosis, plus stroke-like episodes (melas) and acute ischemic stroke (ais). *J Clin Neurosci* 2018; **55**: 65–70: S0967-5868(17)31727-7. https://doi.org/10.1016/j.jocn.2018.06.015
112. Ikawa M, Yoneda M, Muramatsu T, Matsunaga A, Tsujikawa T, Yamamoto T, et al. Detection of preclinically latent hyperperfusion due to stroke-like episodes by arterial spin-labeling perfusion MRI in MELAS patients. *Mitochondrion* 2013; **13**: S1567-7249(13)00251-1: 676–80: . https://doi.org/10.1016/j.mito.2013.09.007
113. Whitehead MT, Lee B, Gropman A. Lesional perfusion abnormalities in leigh disease demonstrated by arterial spin labeling correlate with disease activity. *Pediatr Radiol* 2016; **46**: 1309–16. https://doi.org/10.1007/s00247-016-3616-9
114. Phyu P, Merwick A, Davagnanam I, Bolsover F, Jichi F, Wheeler-Kingshott C, et al. Increased resting cerebral blood flow in adult fabry disease: MRI arterial spin labeling study. *Neurology* 2018; **90**: e1379–85. https://doi.org/10.1212/WNL.0000000000005330
115. Sekar S, Vinayagamani S, Thomas B, Kesavadas C. Arterial spin labeling hyperperfusion in seizures associated with non-ketotic hyperglycaemia: is it merely a post-ictal phenomenon? *Neurol Sci* 2021; **42**: 739–44. https://doi.org/10.1007/s10072-020-04815-6